Electronic Supplementary Material (ESI) for Materials Chemistry Frontiers.

Delicate fabrication of $ZnO/ZnCo_2O_4$ heterojunction HoMS as anode for lithium-ion battery with high-rate capability

Hui Zhang[a], Xin Zhou[a], Yahui Liu[c], Baoxiu Hou[a], Linlin Ma[a], Yuan Liu[a], Haiyan Liu[a], Shuaihua Zhang[a], Zhimin Ao[e], Jianjun Song[b*], Jiangyan Wang[d*], Xiaoxian Zhao[a*]

[a] *Department of Chemistry, College of Science, Hebei Agricultural University, Baoding, 071001, China.*

[b] *College of Physics, Qingdao University, Qingdao 266071, China.*

[c] *National Engineering Research Center of green recycling for strategic metal resources, Institute of Process Engineering, Chinese Academy of Sciences, Beijing 100190, China.*

[d] *State Key Laboratory of Biochemical Engineering, Institute of Process Engineering, Chinese Academy of Sciences, No. 1, Beierjie, Zhongguancun, Beijing, 100190, China.*

[e] *Guangdong-Hong Kong-Macao Joint Laboratory for Contaminants Exposure and Health, Guangzhou Key Laboratory Environmental Catalysis and Pollution Control, Institute of Environmental Health and Pollution Control, Guangdong University of Technology, Guangzhou 510006, China.*

E-mail: lxzhxx@hebau.edu.cn (X. Zhao); jywang@ipe.ac.cn (J. Wang); jianjun.song@qdu.edu.cn (J. Song)

Supporting Information Caption

Figure S1. The TGA of $ZnO/ZnCo_2O_4$ HoMS with different compositions.

Figure S2. The Fourier Transform Infrared Spectrometer (FTIR) of $ZnO/ZnCo_2O_4$ HoMS with different compositions.

Figure S3. The XRD of $ZnO/ZnCo_2O_4$ HoMS with different compositions.

Figure S4. The SEM of $ZnO/ZnCo_2O_4$ D-HoMS-4/1 (a), Q-HoMS-3/1 (b), Q-HoMS-1/1 (c), Q-HoMS-1/2 (d), Qa-HoMS-1/3 (e) and T-HoMS-1/4 (f).

Figure S5. The TEM of $ZnO/ZnCo_2O_4$ D-HoMS-4/1 (a), Q-HoMS-3/1 (b), Q-HoMS-1/1 (c), Q-HoMS-1/2 (d), Qa-HoMS-1/3 (e) and T-HoMS-1/4 (f).

Figure S6. The Zn2p XPS high-resolution analysis of $ZnO/ZnCo_2O_4$ Q-HoMS-2/1.

Figure S7. The O1s XPS high-resolution analysis of $ZnO/ZnCo_2O_4$ Q-HoMS-2/1 (O_C is chemisorbed oxygen), O_V is oxygen vacancies, O_L is lattice oxygen).

Figure S8. The charge-discharge curves of $ZnO/ZnCo_2O_4$ Q-HoMS-3/1 (a), Q-HoMS-2/1 (b), Q-HoMS-1/1 (c) and Q-HoMS-1/2 (d).

Figure S9. The cyclic voltammetry curves of $ZnO/ZnCo_2O_4$ Q-HoMS-3/1 (a), Q-HoMS-2/1 (b), Q-HoMS-1/1 (c) and Q-HoMS-1/2 (d).

Figure S10. The BET curves of $ZnO/ZnCo_2O_4$ Q-HoMS-3/1, Q-HoMS-2/1, Q-HoMS-1/1 and Q-HoMS-1/2.

Figure S11. The calculation results for capacitive contribution at 3 mV s^{-1} scan rate of $ZnO/ZnCo_2O_4$ Q-HoMS-3/1 (a), Q-HoMS-2/1 (b), Q-HoMS-1/1 (c) and Q-HoMS-1/2 (d).

Figure S12. The SEM of $ZnO/ZnCo_2O_4$ S-HoMS-2/1 (a), D-HoMS-2/1 (b), T-HoMS-2/1 (c) and Qa-HoMS-2/1 (d).

Figure S13. The TEM of $ZnO/ZnCo_2O_4$ S-HoMS-2/1 (a), D-HoMS-2/1 (b), T-HoMS-2/1 (c) and Qa-HoMS-2/1 (d).

Figure S14. The rate capability test of $ZnO/ZnCo_2O_4$ S-HoMS-2/1, D-HoMS-2/1, T-HoMS-2/1 and Qa-HoMS-2/1.

Figure S15. The charge-discharge curves of $ZnO/ZnCo_2O_4$ S-HoMS-2/1 (a), D-HoMS-2/1 (b), T-HoMS-2/1 (c) and Qa-HoMS-2/1 (d) at different current densities.

Figure S16. The cyclic voltammetry curves of $ZnO/ZnCo_2O_4$ S-HoMS-2/1 (a), D-HoMS-2/1 (b), T-HoMS-2/1 (c) and Qa-HoMS-2/1 (d) at different scan rates.

Figure S17. The calculation results for capacitive contribution at 3 mV s^{-1} scan rate of $ZnO/ZnCo_2O_4$ S-HoMS-2/1 (a), D-HoMS-2/1 (b), T-HoMS-2/1 (c) and Qa-HoMS-2/1 (d).

Figure S18. The BET curves of $ZnO/ZnCo_2O_4$ S-HoMS-2/1, D-HoMS-2/1, T-HoMS-2/1 and Qa-HoMS-2/1.

Table S1. The mass of cobalt acetate and zinc acetate added to the reaction.

Table S2. The preparing conditions of multi-shelled $ZnO/ZnCo_2O_4$ Q-HoMS-2/1 hollow spheres.

Table S3. Cell parameters and occupied positions of refined $ZnCo_2O_4$.

Table S4. Cell parameters and occupied positions of refined ZnO.

Table S5. Two-phase proportion of ZnO and $ZnCo_2O_4$ and all errors in the refined results.

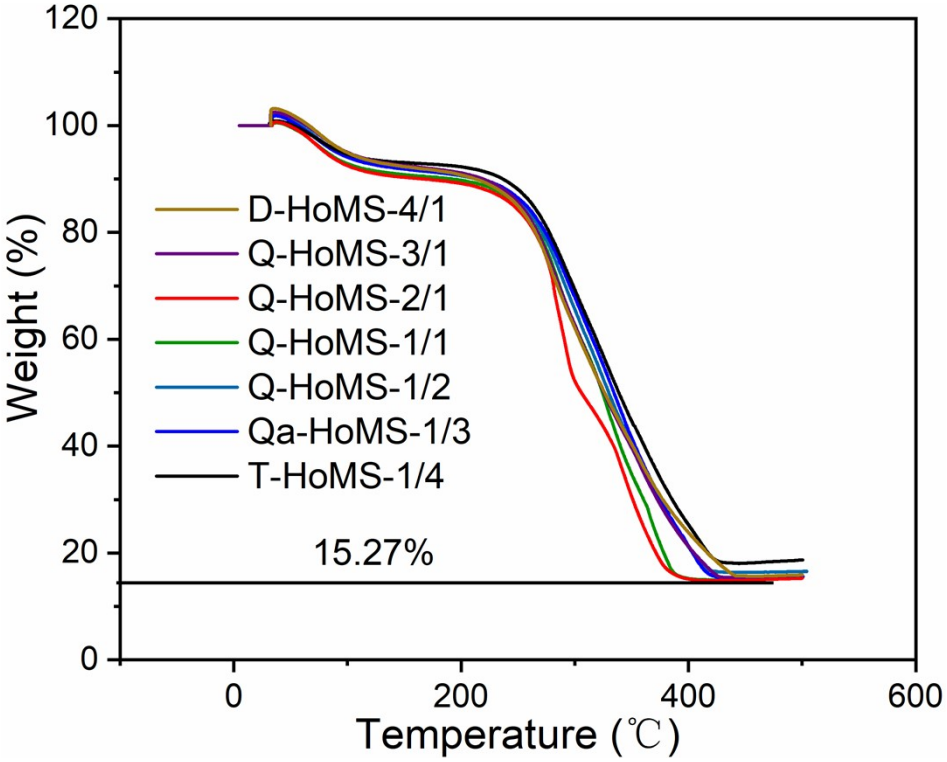

Figure S1. The TGA of ZnO/$ZnCo_2O_4$ HoMS with different compositions.

The combustion rate of carbon sphere was increased first and then decreased with the increase of the molar ratio of Co/Zn.

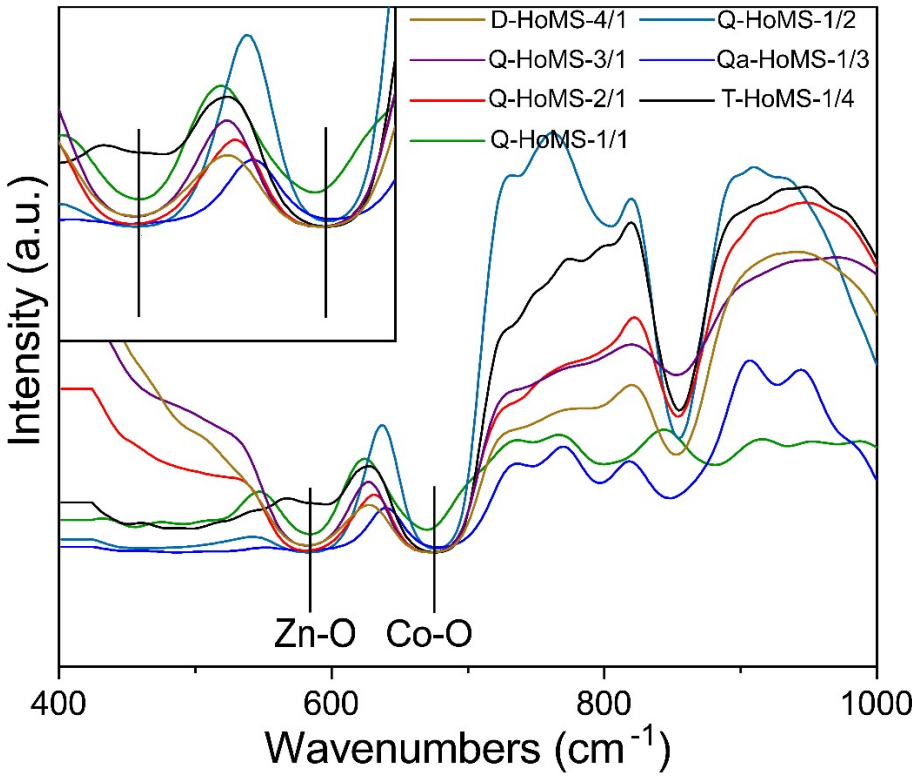

Figure S2. The Fourier Transform Infrared Spectrometer (FTIR) of $ZnO/ZnCo_2O_4$ HoMS with different compositions.

With increasing molar ratio of Co/Zn, the peak position of Co-O bond corresponding to stretching vibration in Fourier Transform Infrared Spectrometer (FTIR) was decreased.

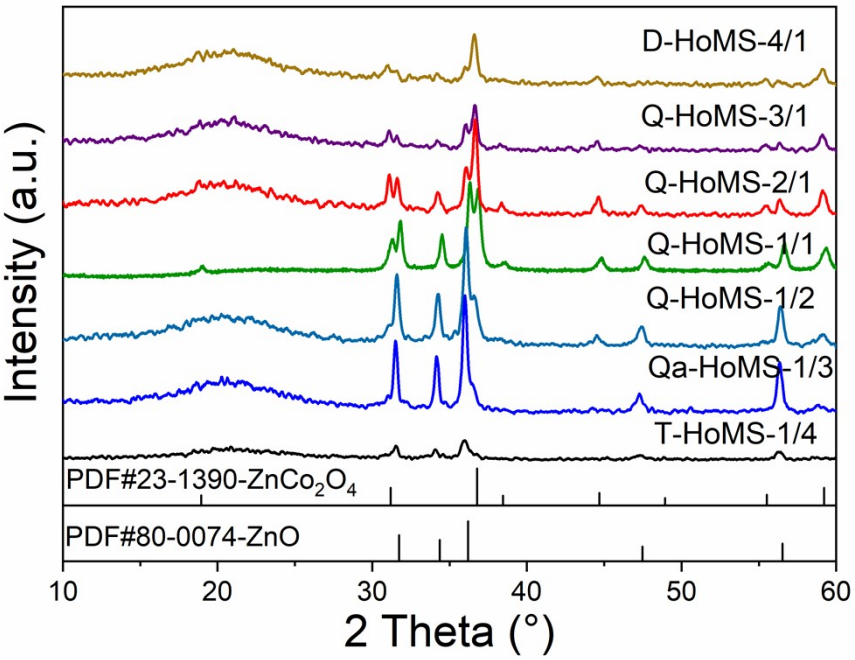

Figure S3. The XRD of ZnO/$ZnCo_2O_4$ HoMS with different compositions.

With increasing molar ratio of Co/Zn, the peak intensity standing for $ZnCo_2O_4$ in XRD was increased and the peak intensity corresponding to ZnO was decreased.

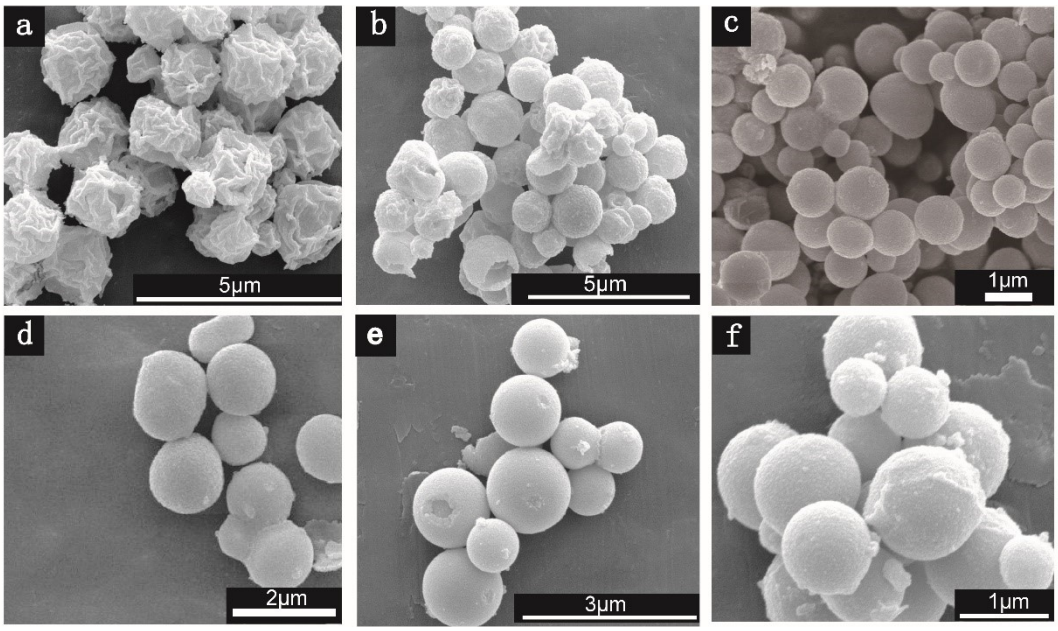

Figure S4. The SEM of $ZnO/ZnCo_2O_4$ D-HoMS-4/1 (a), Q-HoMS-3/1 (b), Q-HoMS-1/1 (c), Q-HoMS-1/2 (d), Qa-HoMS-1/3 (e) and T-HoMS-1/4 (f).

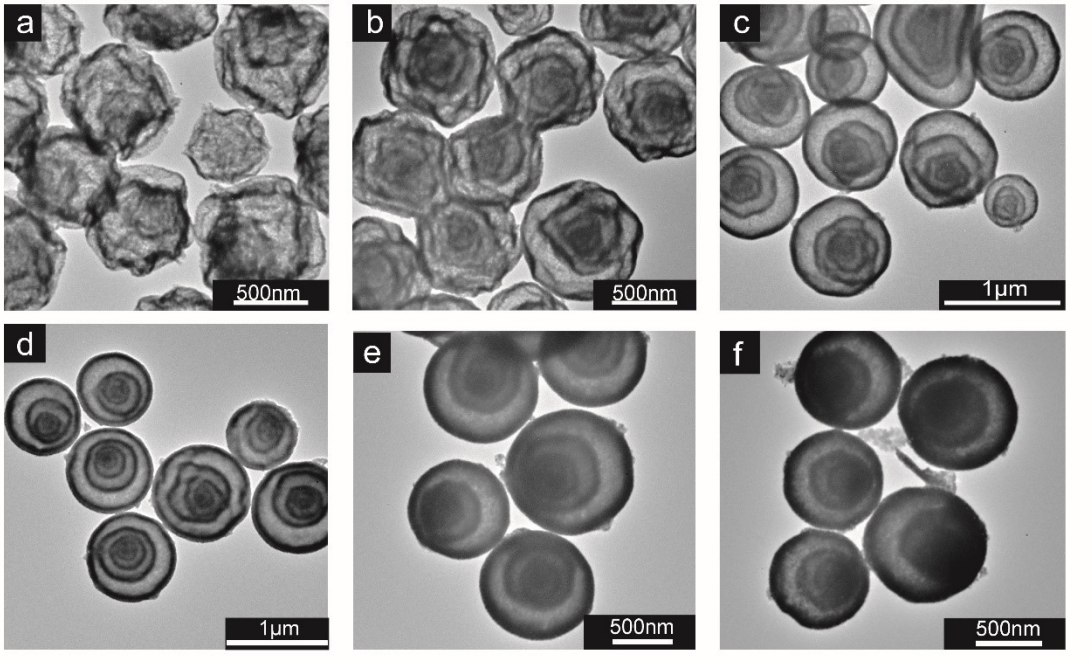

Figure S5. The TEM of $ZnO/ZnCo_2O_4$ D-HoMS-4/1 (a), Q-HoMS-3/1 (b), Q-HoMS-1/1 (c), Q-HoMS-1/2 (d), Qa-HoMS-1/3 (e) and T-HoMS-1/4 (f).

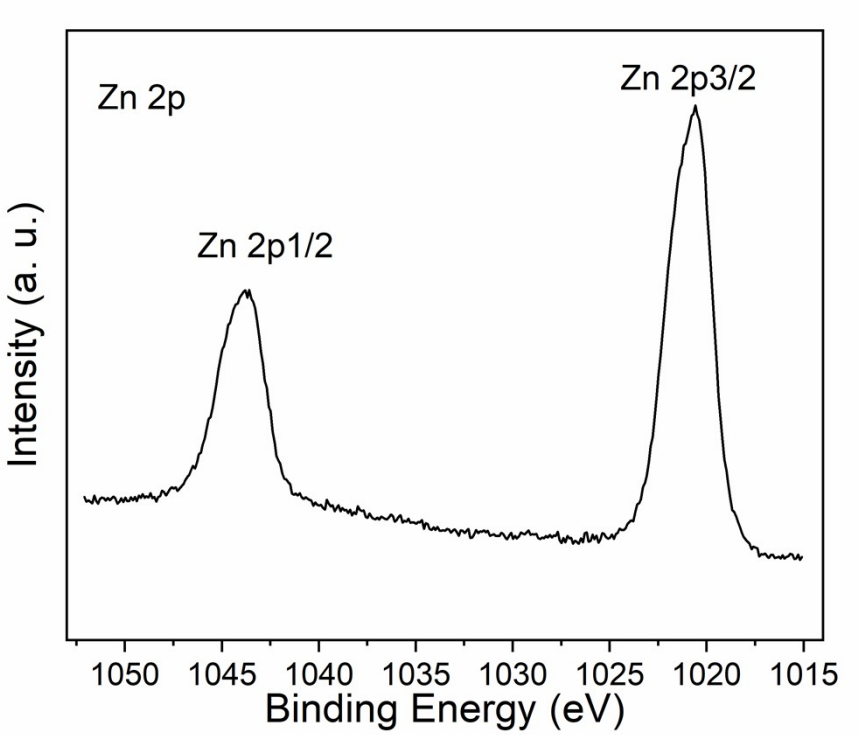

Figure S6. The Zn2p XPS high-resolution analysis of $ZnO/ZnCo_2O_4$ Q-HoMS-2/1.

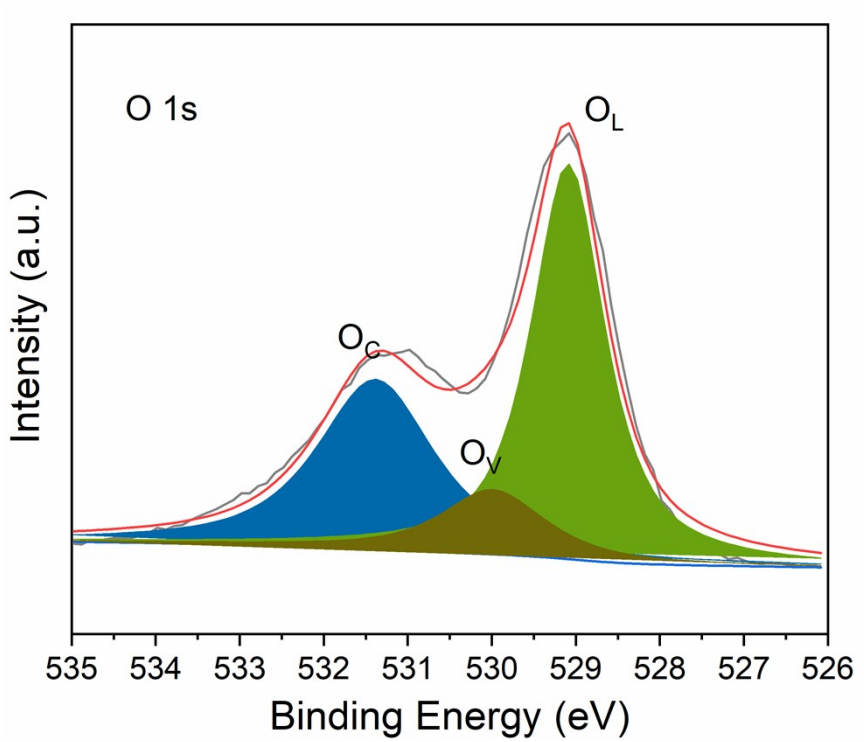

Figure S7. The O1s XPS high-resolution analysis of $ZnO/ZnCo_2O_4$ Q-HoMS-2/1 (O_C is chemisorbed oxygen), O_V is oxygen vacancies, O_L is lattice oxygen).

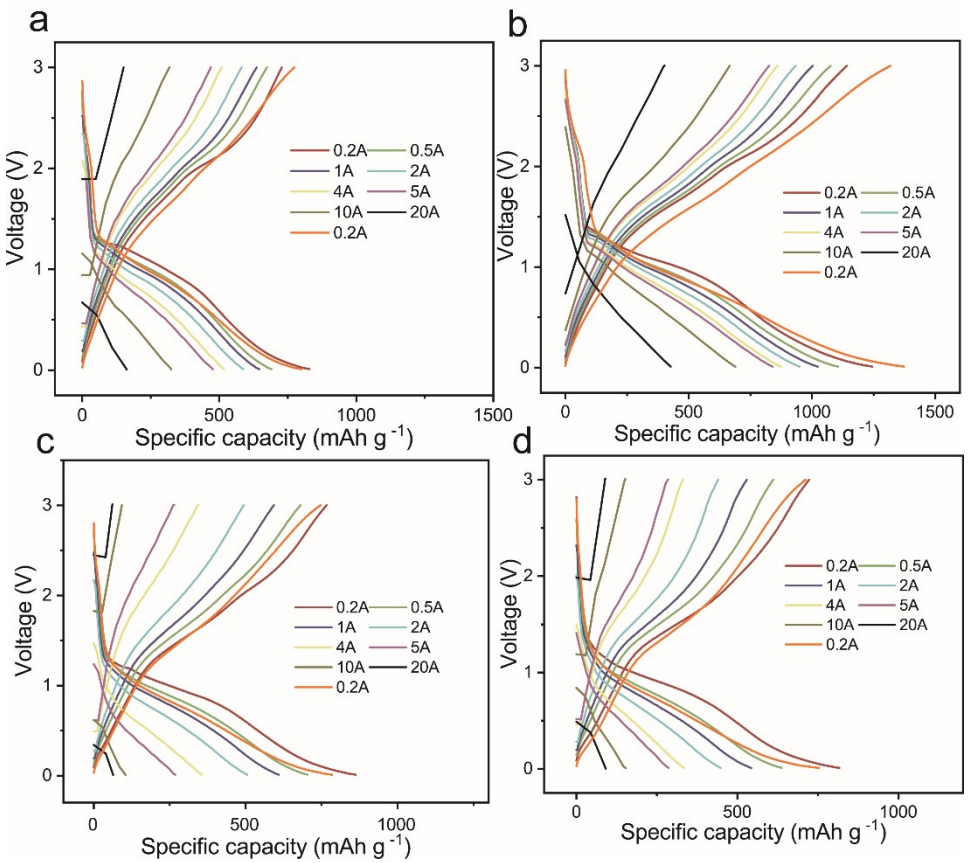

Figure S8. The charge-discharge curves of $ZnO/ZnCo_2O_4$ Q-HoMS-3/1 (a), Q-HoMS-2/1 (b), Q-HoMS-1/1 (c) and Q-HoMS-1/2 (d).

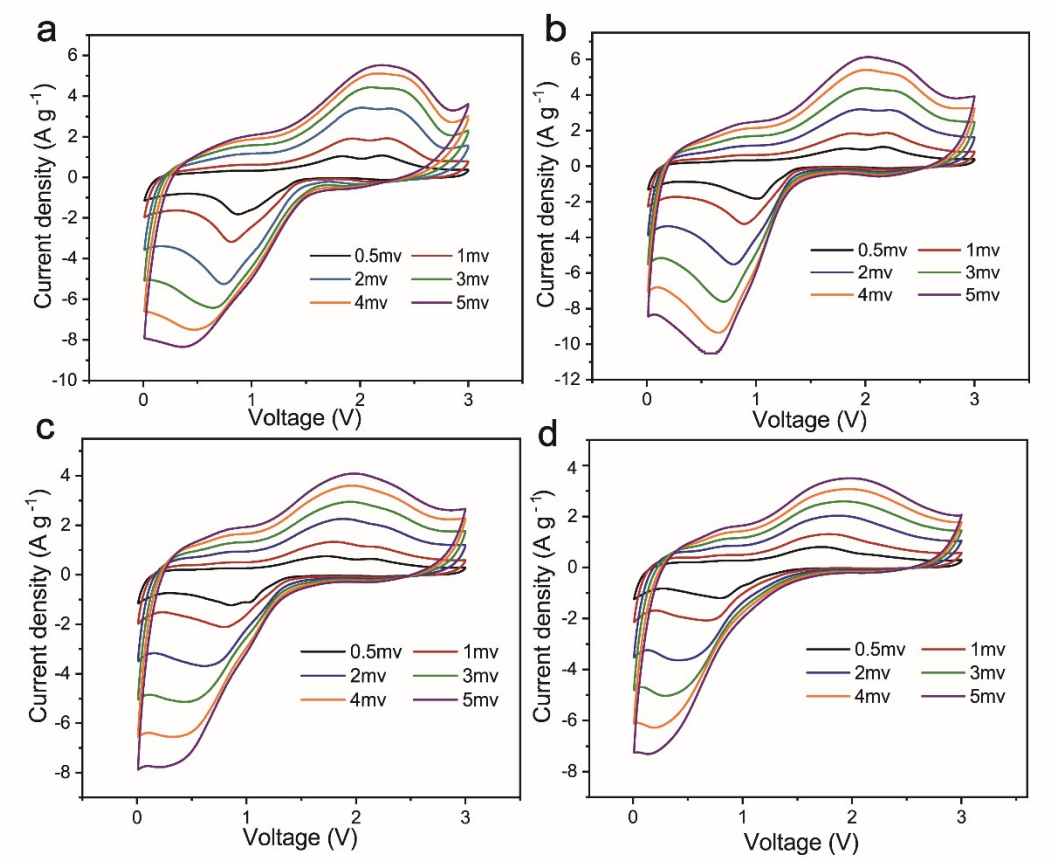

Figure S9. The cyclic voltammetry curves of $ZnO/ZnCo_2O_4$ Q-HoMS-3/1 (a), Q-HoMS-2/1 (b), Q-HoMS-1/1 (c) and Q-HoMS-1/2 (d).

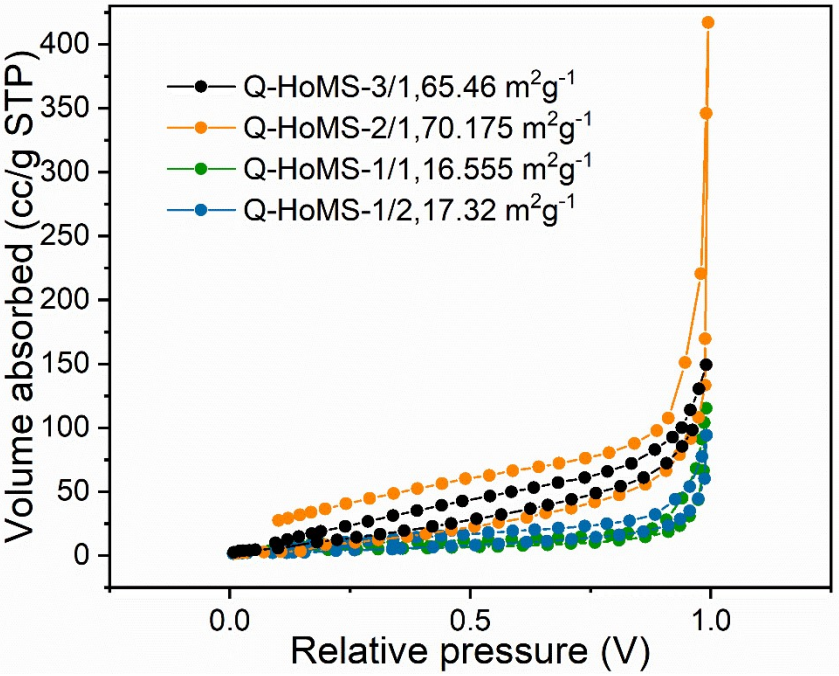

Figure S10. The BET curves of $ZnO/ZnCo_2O_4$ Q-HoMS-3/1, Q-HoMS-2/1, Q-HoMS-1/1 and Q-HoMS-1/2.

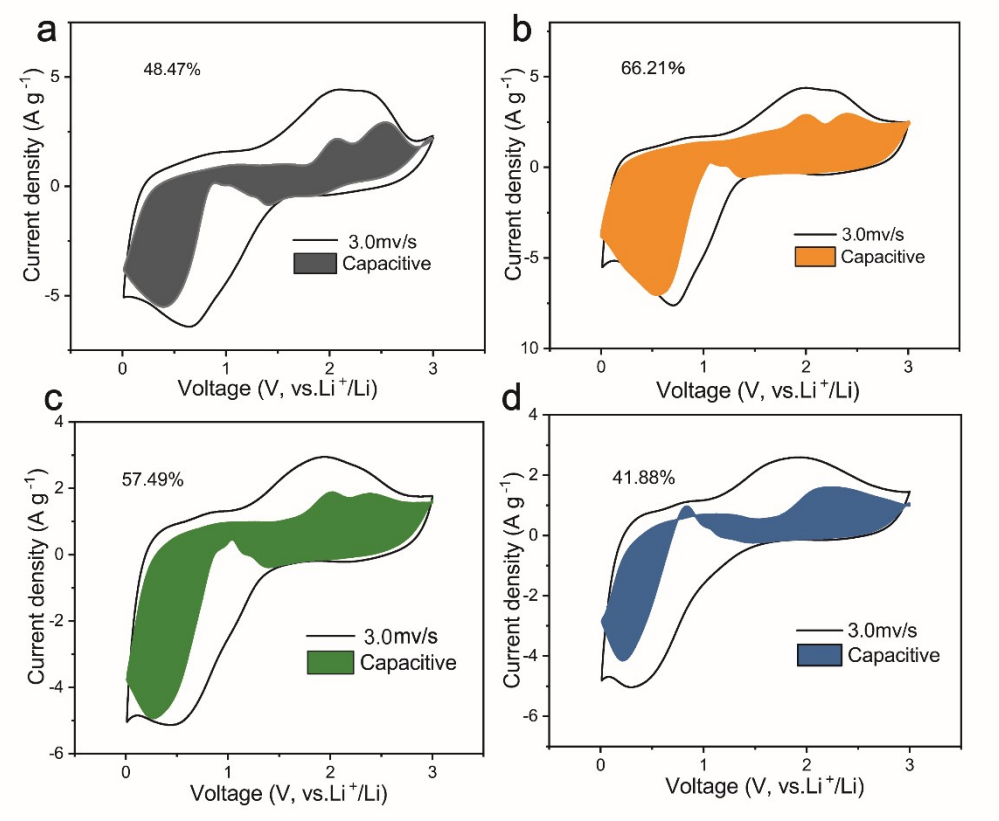

Figure S11. The calculation results for capacitive contribution at 3 mV s^{-1} scan rate of $ZnO/ZnCo_2O_4$ Q-HoMS-3/1 (a), Q-HoMS-2/1 (b), Q-HoMS-1/1 (c) and Q-HoMS-1/2 (d).

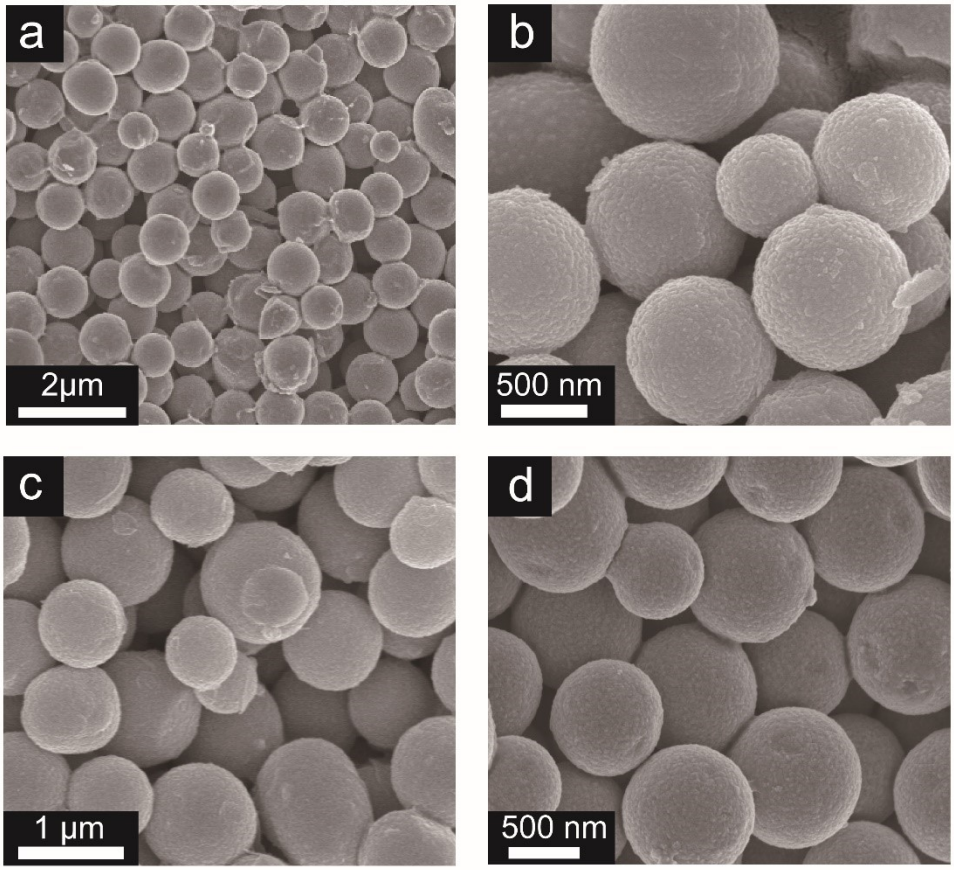

Figure S12. The SEM of $ZnO/ZnCo_2O_4$ S-HoMS-2/1 (a), D-HoMS-2/1 (b), T-HoMS-2/1 (c) and Qa-HoMS-2/1 (d).

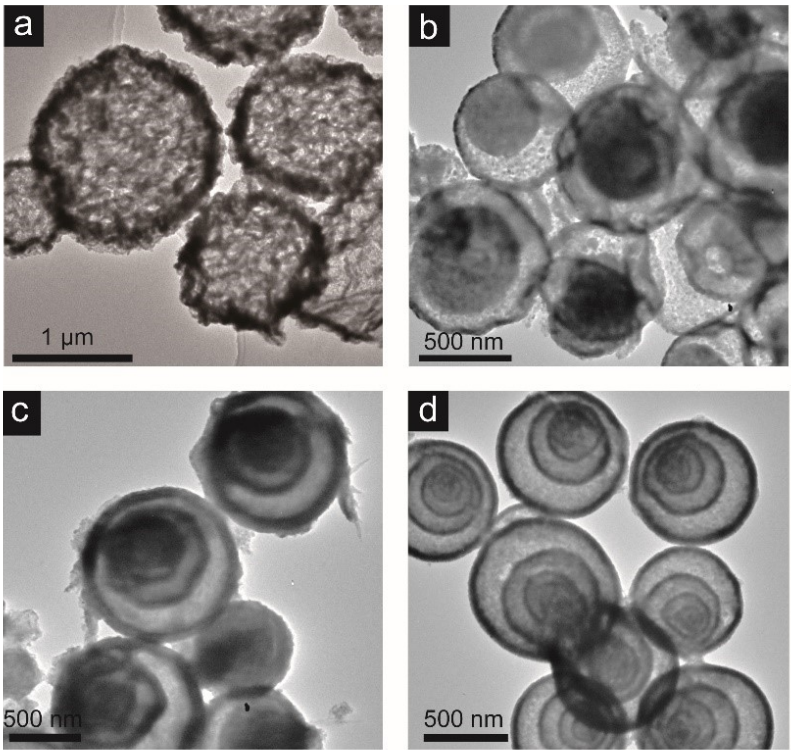

Figure S13. The TEM of $ZnO/ZnCo_2O_4$ S-HoMS-2/1 (a), D-HoMS-2/1 (b), T-HoMS-2/1 (c) and Qa-HoMS-2/1 (d).

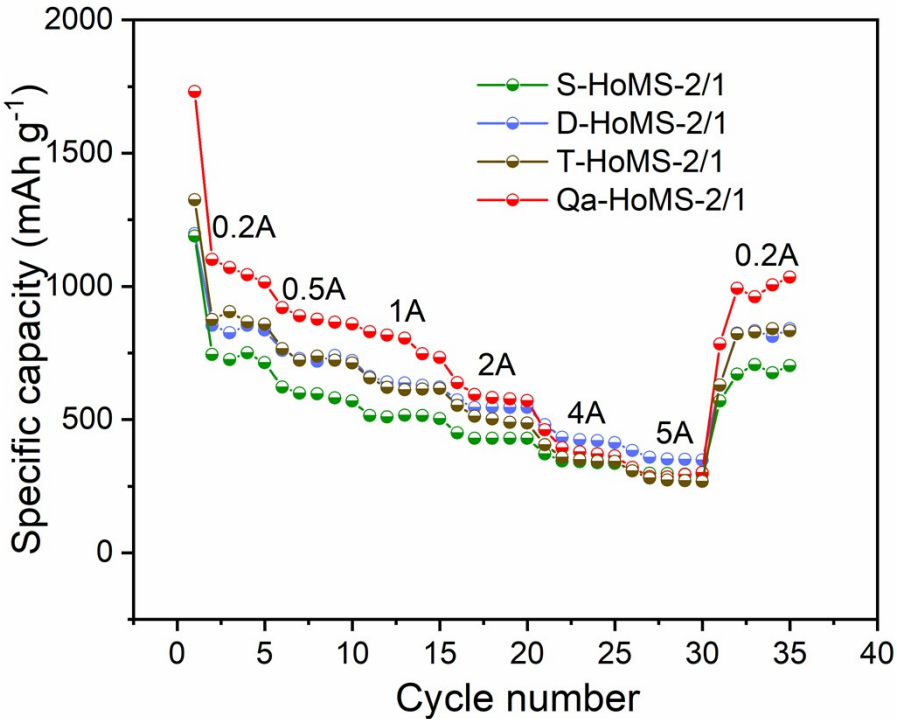

Figure S14. The rate capability test of $ZnO/ZnCo_2O_4$ S-HoMS-2/1, D-HoMS-2/1, T-HoMS-2/1 and Qa-HoMS-2/1.

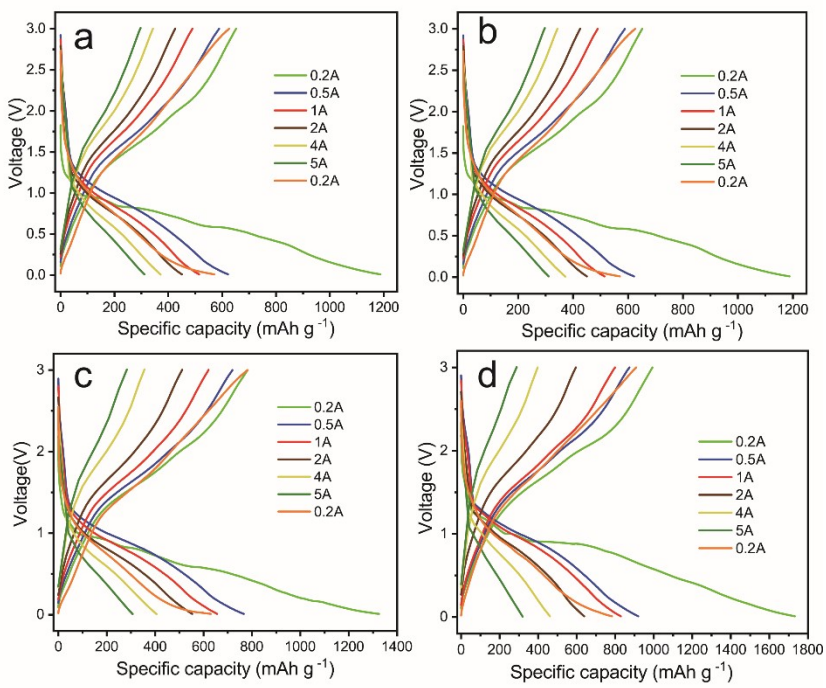

Figure S15. The charge-discharge curves of ZnO/$ZnCo_2O_4$ S-HoMS-2/1 (a), D-HoMS-2/1 (b), T-HoMS-2/1 (c) and Qa-HoMS-2/1 (d) at different current densities.

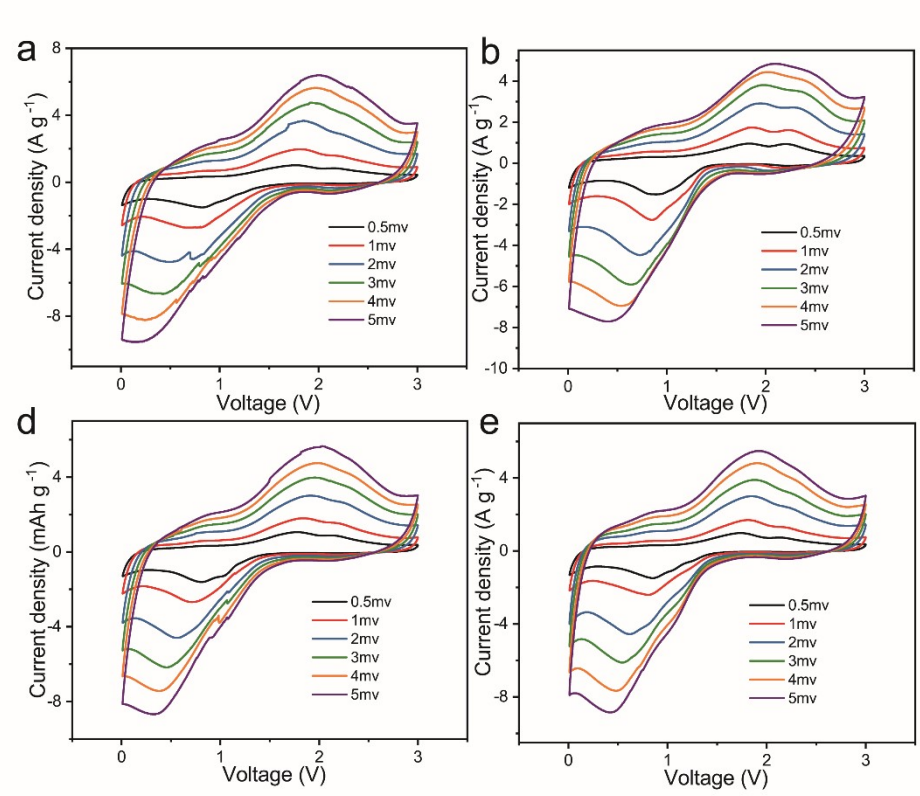

Figure S16. The cyclic voltammetry curves of $ZnO/ZnCo_2O_4$ S-HoMS-2/1 (a), D-HoMS-2/1 (b), T-HoMS-2/1 (c) and Qa-HoMS-2/1 (d) at different scan rates.

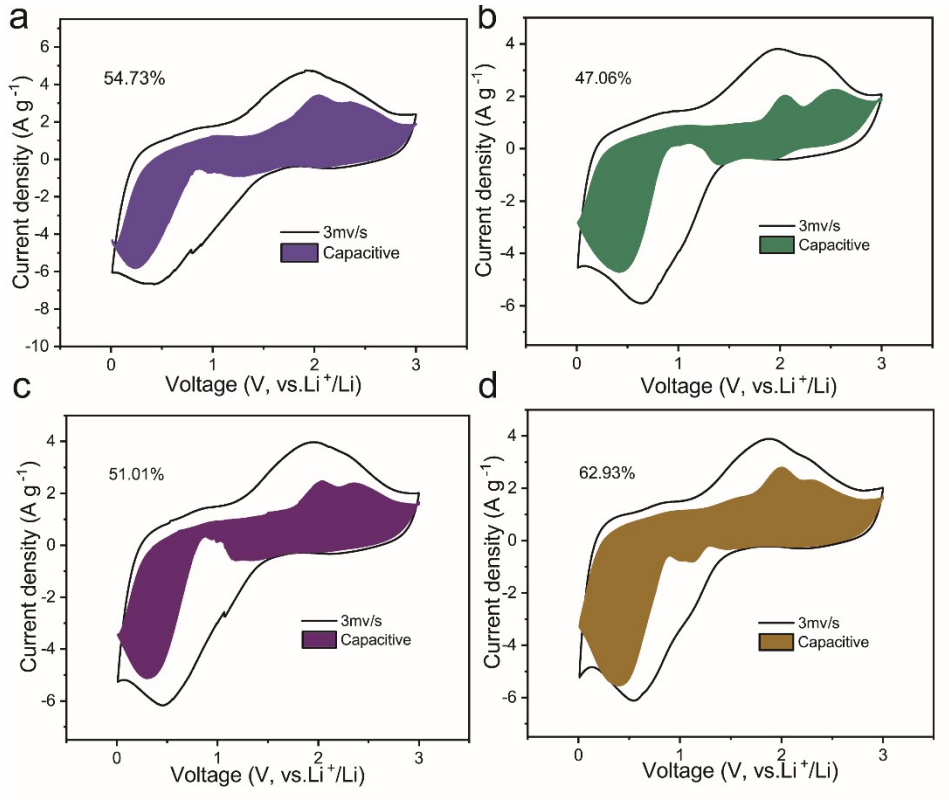

Figure S17. The calculation results for capacitive contribution at 3 mV s^{-1} scan rate of $ZnO/ZnCo_2O_4$ S-HoMS-2/1 (a), D-HoMS-2/1 (b), T-HoMS-2/1 (c) and Qa-HoMS-2/1 (d).

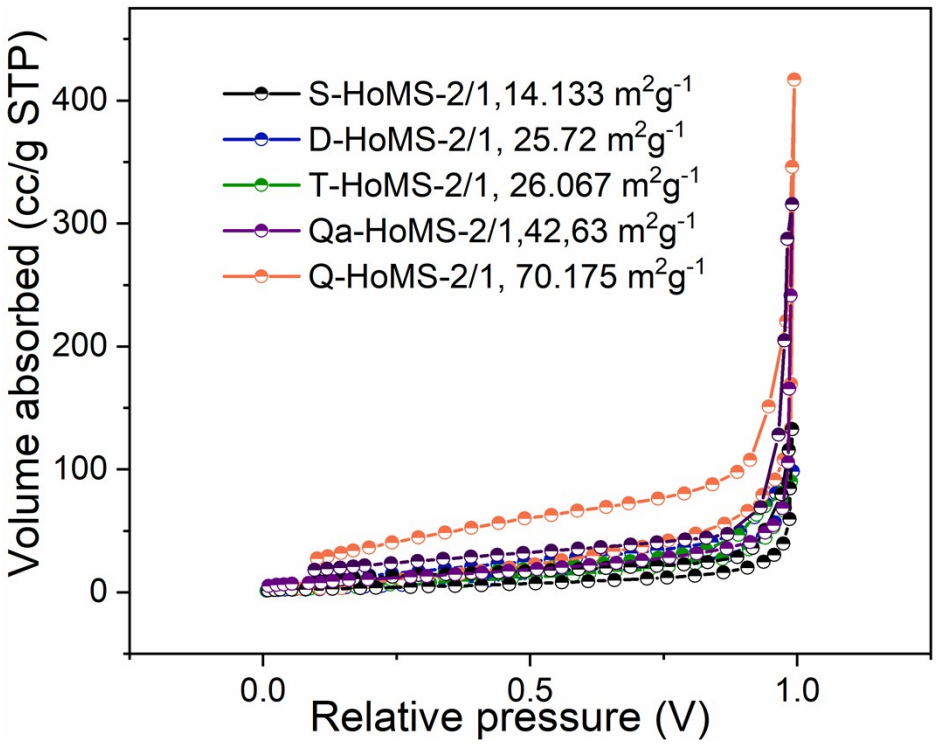

Figure S18. The BET curves of ZnO/$ZnCo_2O_4$ S-HoMS-2/1, D-HoMS-2/1, T-HoMS-2/1, Qa-HoMS-2/1 and Q-HoMS-2/1.

Table S1. The mass of cobalt acetate and zinc acetate added to the reaction.

the molar ratio of Co/Zn	Cobalt acetate (g)	Zinc acetate (g)
1v1	1.49	1.32
1v2	0.75	1.32
1v3	0.75	1.98
1v4	0.75	2.63
2v1	1.49	0.66
3v1	2.24	0.66
4v1	2.99	0.66

Table S2. The preparing conditions of multi-shelled $ZnO/ZnCo_2O_4$ Q-HoMS hollow spheres.

	temperature (ºC)	time (h)	Molar ratio of ethanol to water	Heating speed (°C/min)	Zinc acetate (g)	Cobalt acetate (g)
Single	30	3	0	1	0.66	1.49
Double	30	3	3	1	0.66	1.49
Triple	30	12	0	1	0.66	1.49
Quadruple	30	6	3	1	0.66	1.49
Quintuple	30	12	3	1	0.66	1.49

Table S3. Cell parameters and occupied positions of refined $ZnCo_2O_4$.

type	Ref/damp	Fractional coordinates	Mult	Occupancy
O	0 0 0	-0.12819 -0.12819 -0.12819	16	1.0000
O	0 0 0	0.37819 0.37819 0.37819	16	1.0000
ZN	0 0 0	0.62500 0.62500 0.62500	16	1.0000
CO	0 0 0	0.25000 0.25000 0.25000	4	1.0000
CO	0 0 0	0.00000 0.00000 0.00000	4	1.0000

Table S4. Cell parameters and occupied positions of refined ZnO.

type	Ref/damp	Fractional coordinates	Mult	Occupancy
ZN+2	0 0 0	0.3333 0.6667 0.0000	2	1.0000
O-2	0 0 0	0.3333 0.6667 0.3750	2	1.0000

Table S5. Two-phase proportion of ZnO and $ZnCo_2O_4$ and all errors in the refined results.

Fitted		-Bknd		
wRp	Rp	wRp	Rp	DWd
0.0175	0.0134	0.0234	0.0183	0.477
0.0175	0.0134	0.0234	0.0183	0.477